Available online at www.sciencedirect.com

ScienceDirect

IFAC PapersOnLine 56-2 (2023) 4436–4441

Data selection and data-enabled predictive control for a fuel cell system

Lukas Schmitt * **Julius Beerwerth** * **Dirk Abel** *

* *Institute of Automatic Control, RWTH Aachen University, 52072 Aachen, Germany (e-mail: l.schmitt@ irt.rwth-aachen.de).*

Abstract: Data-enabled predictive control is applied for power tracking of a fuel cell system and algorithmic aspects are investigated. For the system realization, the column subset selection algorithms norm sampling, iterative norm sampling, leverage score sampling, and selection based on the strong rank-revealing QR factorization are compared. Regularization using the 1-norm and the squared 2-norm on the column combination vector g is evaluated in terms of runtime and closed-loop results. The results indicate that column selection based on a strong rank-revealing QR (sRRQR) decomposition and leverage score sampling lead to consistently small closed-loop costs even with comparatively few columns in the data matrix resulting in reduced computation time. The closed-loop performance with 1-norm and squared 2-norm is similar, with lower turnaround times for the latter.

Keywords: Data-driven optimal control, predictive control, real-time optimal control, optimal operation and control of power systems, fuel cell systems

1. INTRODUCTION

Complex systems with multiple inputs and multiple outputs, operational or safety constraints, and nonlinearities are often controlled by model-based predictive control algorithms. In the standard model predictive control (MPC) approach, a mathematical system model suited for gradient-based optimization is identified first and subsequently used in the control algorithm. System identification can be cumbersome and the fitness of a model in closed-loop control can only be analyzed afterward, such that an iteration of system identification and closed-loop testing might occur. Additionally, expert knowledge for deriving physics-based models is essential. In contrast to that, direct data-driven methods bypass the explicit identification step and directly use data to derive the control policy, for a survey see (Hou and Wang, 2013). An example of direct data-driven control, that recently gained traction is data-enabled predictive control (DeePC) (Coulson et al., 2019b). Similarly to MPC, an optimization problem is set up and solved in a receding horizon fashion, composed of a cost function encoding the control task and of constraints defining the operational limits. The prediction of DeePC, however, relies solely on input-output trajectories of the underlying unknown system (Markovsky and Rapisarda, 2008). Based on the Fundamental Lemma in behavioral system theory for linear time-invariant (LTI) systems, the collected trajectories span the subspace of all possible system trajectories if the corresponding input is persistently exciting (Willems et al., 2005). This approach was proven to be equivalent to subspace predictive control for LTI systems (Fiedler and Lucia, 2020). Theoretic guarantees such as open-loop and closed-loop robustness properties (Coulson et al., 2020), (Berberich et al., 2020), exponential stability for setpoint-tracking in closed-loop (Berberich et al., 2021b), and others are established analogously to MPC (Berberich et al., 2021a).

While for underlying LTI systems, theoretic foundations have been developed quickly, equivalent results are harder to achieve for nonlinear systems. Nevertheless, this approach has also been applied successfully to challenging real-world problems, such as control of grid-connected power converters (Coulson et al., 2019a), quadrocopter (Elokda et al., 2019), synchronous motor drives (Carlet et al., 2020), and tank systems (Berberich et al., 2021a). In this paper, we use DeePC to control a nonlinear fuel cell system model for net power output tracking. Focusing on real-world applicability for resource-constrained embedded hardware, several data selection algorithms from literature are applied to find the most informative system description with limited data. The algorithms are evaluated in closed loop. Turnaround times on a rapid control prototyping hardware are reported for the 1-norm and squared 2-norm regularization of the linear combination of data trajectories.

The remainder of the paper is structured as follows. The basic algorithmic components of DeePC in Section 2 and established procedures for column subset selection are revised and adapted to the problem at hand in Section 3. The fuel cell system plant model is detailed in Section 4 and results are presented in Section 5.

2. DATA-ENABLED PREDICTIVE CONTROL

2.1 Preliminaries

Theoretical results in the context of the DeePC algorithm rely on an underlying LTI system with inputs $u_k \in \mathbb{R}^m$ and outputs $y_k \in \mathbb{R}^p$. For a sequence $u = \{u_k\}_{k=1}^T$, we define the Hankel matrix with L block rows as

$$H_L(u) = \begin{bmatrix} u_1 & u_2 & \dots & u_{T-L+1} \\ u_2 & u_3 & \dots & u_{T-L+2} \\ \vdots & \vdots & \ddots & \vdots \\ u_L & u_{L+1} & \dots & u_T \end{bmatrix}. \tag{1}$$

Definition 1. (Persistency of Excitation, (Willems et al., 2005)). A sequence of signals $u = \{u_k\}_{k=1}^T$ is called persistently excit-

10.1016/j.ifacol.2023.10.1835

ing of order L if the Hankel matrix $H_L(u)$ has full row rank, i. e. $\text{rank}(H_L(u)) = mL$.

For the matrix $H_L(u)$ to have full row rank, the length of the initial trajectory is bounded by $T \geq (m+1)L-1$, where n is the state dimension of the underlying LTI system (Coulson et al., 2019b).

Theorem 1. Suppose $\{u_k, y_k\}_{k=1}^{T}$ is a trajectory of an LTI system G, where u is persistently exciting of order $L+n$. Then, $\{\bar{u}_k, \bar{y}_k\}_{k=1}^{L}$ is a trajectory of G if and only if there exists $g \in \mathbb{R}^{T-L+1}$ such that

$$\begin{bmatrix} H_L(u) \\ H_L(y) \end{bmatrix} g = \begin{bmatrix} \bar{u} \\ \bar{y} \end{bmatrix}. \tag{2}$$

According to this theorem, originally from (Willems et al., 2005), adapted in (Elokda et al., 2019), all trajectories of an unknown LTI system can be constructed from a single persistently exciting trajectory. Equivalently, the subspace spanned by the columns of the Hankel matrix corresponds exactly to the subspace of possible trajectories of the underlying LTI system.

If the Hankel matrix in (2) is further divided into past and future data, denoted by subscripts p and f respectively, (3) results, where $U_p \in \mathbb{R}^{mT_{\text{ini}} \times (T-L+1)}$, $Y_p \in \mathbb{R}^{pT_{\text{ini}} \times (T-L+1)}$, $Y_f \in \mathbb{R}^{pN \times (T-L+1)}$, $U_f \in \mathbb{R}^{mN \times (T-L+1)}$. Hence the partitioning is according to T_{ini} past steps and N predictive steps. Given the past sequences u_{ini}, y_{ini}, and a future input sequence $u = \{u_k\}_{k=1}^{N}$, the first three blocks can be used to calculate g. The output prediction results from the last block as $Y_f g = y$, where $y = \{y_k\}_{k=1}^{N}$.

$$\begin{bmatrix} U_p \\ Y_p \\ U_f \\ Y_f \end{bmatrix} g = \begin{bmatrix} u_{\text{ini}} \\ y_{\text{ini}} \\ u \\ y \end{bmatrix} \tag{3}$$

It has been found that the originally used Hankel structure is not required for DeePC, but rather any column-wise trajectory matrix can be used (Coulson et al., 2020).

2.2 Regularized DeePC

Similarly to MPC, an optimization problem is solved in the DeePC algorithm in a receding horizon fashion in order to calculate the optimal inputs at each time step. The cost function consists of a tracking term for the output y, a penalty on Δu for smooth input trajectories, and additional regularization terms. Instead of using a parametric system representation derived through an identification procedure, the system's behavioral description is composed solely of past data trajectories, measured from the unknown system. With the equality constraint (4b), implicit state estimation and prediction are established. Even for LTI systems, noisy measurements in Y_p and y_{ini} render the implicit state estimation potentially inconsistent. In order to maintain consistent and smooth implicit state estimates, the equality constraint $Y_p g = y_{\text{ini}} + \sigma$ is relaxed by the slack variable $\sigma \in \mathbb{R}^{pT_{\text{ini}}}$ which is penalized in the cost function. This softening coincidences roughly with a least-squares estimate of the initial condition (Elokda et al., 2019). It is reported in the literature (e.g. Elokda et al., 2019), that the penalty λ_y on σ should be chosen large without affecting the numerical properties of the optimization too much. The optimization variable g determines the system behavior through a linear combination of the trajectory columns. Regularization on g can be added to avoid over-fitting and increase robustness, which was later rigorously connected to distributionally robust optimization (Coulson et al., 2019c). For the penalty λ_g on g, optimal plateaus are observed, balancing the prediction error and model flexibility.

$$\min_{g,u,y,\sigma} \quad \sum_{k=1}^{N} \|y_k - r_k\|_2^2 + \sum_{k=0}^{N-1} \|\Delta u_k\|_2^2 + \lambda_g \|g\| + \lambda_y \|\sigma\|_2^2 \tag{4a}$$

$$\text{s. t.} \quad \begin{bmatrix} U_p \\ Y_p \\ U_f \\ Y_f \end{bmatrix} g = \begin{bmatrix} u_{\text{ini}} \\ y_{\text{ini}} \\ u \\ y \end{bmatrix} + \begin{bmatrix} 0 \\ \sigma \\ 0 \\ 0 \end{bmatrix} \tag{4b}$$

$$u_k \in \mathbb{U}, \quad \forall k \in \{0, ..., N-1\} \tag{4c}$$

$$y_k \in \mathbb{Y}, \quad \forall k \in \{1, ..., N\} \tag{4d}$$

While, in general, any norm can be used, the 1-norm and squared 2-norm represent a sparse solution vector g and a balanced combination vector g respectively, are established in the literature. Using the squared 2-norm leads to an increasingly balanced use of the trajectories with increasing λ_g. From an optimization point of view, this regularization does not introduce additional optimization variables such that the computational complexity for the underlying QP solver remains roughly constant. Using an 1-norm regularization, on the other hand, leads to a sparse vector g, where sparsity depends on the penalty λ_g. This corresponds to selecting only a few suitable trajectories for describing the system behavior using the immediate past data u_{ini} and y_{ini}. Reformulation of the 1-norm regularization into standard QP-form, however, introduces $T-L+1$ additional optimization variables. Thus, increasing the size of the data matrix also yields an increase in complexity and memory requirement compared to the squared 2-norm regularization. As in standard MPC, constraints on the inputs u including the change of input Δu and outputs y encoded in the sets $\mathbb{U}$ and $\mathbb{Y}$ can be added, see (4c) and (4d).

2.3 Practical Considerations

When facing real-world problems, the essential assumption of an underlying LTI system is often invalid. As a consequence, persistence of excitation in the sense of generating an output sequence that is representative of the system's behavior cannot be guaranteed. Even with a rich initial data set and a Hankel matrix with full row rank, ensuring an adequate system representation through data trajectories is a major challenge for nonlinear systems. In addition, when running the algorithm on resource-constrained embedded hardware, the system representation must be compact to reduce the impact on memory and optimization runtime. Naturally, the question of appropriate data collection and data selection arises.

3. DATA SELECTION

Given a measured input-output trajectory of the unknown underlying system, the Hankel matrix for system representation according to behavioral system theory can be constructed. In practice, the initial data collection is often not restricted to a minimal time span, such that a significantly longer trajectory than the theoretic limit for LTI systems can be recorded and a bigger Hankel matrix with more columns $T-L+1$ can be constructed. The optimization problem, however, has $(T-L)+1+(m+p)N+pT_{\text{ini}}$ optimization variables, such that an excessive sequence length T prohibits the use of DeePC in real-time applications and on memory-constrained hardware.

3.1 Column Subset Selection Algorithms

In this work, we investigate column subset selection algorithms (CSS) that are established to build low-rank approximations of large data matrices using the actual columns in contrast to the singular value decomposition. Furthermore, we seek to identify a subset of columns of size n_c that is larger than the number of rows of the data matrix. Whenever necessary, we adapt the CSS algorithms to an iterative procedure by removing the selected columns from the Hankel matrix before running the algorithms again on the smaller matrix. Specifically, the deterministic variants of norm sampling (Algorithm 1), iterative norm sampling (Algorithm 2), leverage score sampling (Algorithm 3), sampling based on the strong rank-revealing QR (sRRQR) decomposition and, for reference, random sampling for the normalized Hankel data matrix $H_L \in \mathbb{R}^{n_1 \times n_2}$ with $n_1 = L(m+p)$ and $n_2 = T-L+1$ are investigated (Wang and Singh, 2015). The algorithms and their computational complexity are shortly revised in the following.

Norm sampling is the simplest and fastest of the sampling algorithms, with a time complexity of $\mathcal{O}(n_1 n_2)$ (Wang and Singh, 2015). The deterministic variant of this algorithm selects the n_c columns with the largest squared 2-norm.

Algorithm 1 Deterministic norm sampling

Input: data matrix H_L, size of column subset n_c

Norm computation: $\hat{c}_i = \|H_L^{(i)}\|_2^2$, $\hat{f} = \sum_i \hat{c}_i$

Selection: $C^{(j)} = H_L{}^{(i)}$, $i = \text{maxind}(\hat{c}/\hat{f}, n_c)$

Output: selected columns C

Iterative norm sampling selects columns from a modified data matrix based on the column's squared 2-norm. In between iterations, the projection of the input matrix onto the column space spanned by the already selected columns $CC^{\dagger}H_L$ is subtracted from the input matrix H_L. When C has full rank, the selected columns are removed from H_L, and Algorithm 2 is executed again until n_c columns are selected. The time complexity is $\mathcal{O}(n_1 n_2 n_c)$ (Wang and Singh, 2015).

Algorithm 2 Iterative norm sampling

Input: data matrix H_L, size of column subset n_c

Initialize: $C = 0$, $X = H_L$

for $j = 1$ to n_c **do**

Norm computation: $\hat{c}_i = \|X^{(i)}\|_2^2$; $\hat{f} = \sum_i \hat{c}_i$

Selection: $C^{(j)} = H_L{}^{(i)}, i = \text{maxind}(\hat{c}/\hat{f})$

Back projection: $X \leftarrow X - CC^{\dagger}X$

end for

Output: selected columns C

Leverage score sampling selects columns based on the squared 2-norm of the top-k truncated right singular vectors and exhibits a complexity of $\mathcal{O}(n_1 n_2 k)$ due to the truncated Singular Value Decomposition (SVD). Leverage scores measure how important a column is in composing the column space.

Lastly, a strong rank-revealing QR decomposition is applied, which generates a specific RRQR decomposition based on column pivoting. The sRRQR algorithm exhibits cubic runtime and produces a similar result to SVD while selecting actual columns of the data matrix. Implementation details and pseudocode can be found in (Chan, 1987) and (Gu and Eisenstat, 1996). The sRRQR algorithm is executed repeatedly until the given number of columns is selected.

Algorithm 3 Deterministic leverage score sampling

Input: data matrix H_L, size of column subset n_c, target rank k

Truncated SVD: $H_L = U_k \Sigma_k V_k^T + R$

Leverage score computation: $l_i = \|V_k^T e_i\|_2^2$

Selection: $C^{(i)} = H_L{}^{(j)}$, $j = \text{maxind}(l, n_c)$

Output: selected columns C

3.2 Evaluation of CSS Algorithm

It has been shown in (Fiedler and Lucia, 2020), that the DeePC equality constraint (4b) can be reformulated for LTI systems as

$$y = P^* \begin{bmatrix} y_{\text{ini}} \\ u_{\text{ini}} \\ u \end{bmatrix}, \tag{5}$$

where the predictor P^* solves the least-squares problem in Frobenius norm $\|.\|_F$

$$P^* = \arg\max_P \|P \underbrace{\begin{bmatrix} Y_p \\ U_p \\ U_f \end{bmatrix}}_{M} - Y_f\|_F^2. \tag{6}$$

For nonlinear systems, the prediction error

$$e = \|P^* M - Y_f\|_F^2 \tag{7}$$

can be compared for different CSS algorithms and a varying number of selected columns of M to calculate P^*. Similar to an open-loop model evaluation in MPC, (7) can serve as an a priori indicator for closed-loop control performance.

4. APPLICATION: FUEL CELL SYSTEM

In this section, the fuel cell system plant model is detailed. The chosen zero-order modeling approach is largely based on (Pukrushpan et al., 2004) and results in a nonlinear model. We assume air is the only species flowing through the cathode since passive humidification is considered to be sufficient. The schematic three tank model is depicted in Fig 1. Manipulated variables are the compressor speed, both throttle valve actuations and the stack current. Controlled outputs are the surge distance of the compressor, the oxygen-hydrogen stoichiometry in the stack and the net power output.

4.1 Compressor Model

The dynamics for the compressor speed n_{cp} are approximated using a second-order lag element. Isentropic compressor efficiency η_{cp} is fitted as a static function of mass flow through the compressor $\dot{m}_{\text{cp}}$ and pressure ratio $\Pi = p_{\text{d}}/p_{\text{u}}$ over the compressor. Consequently, the temperature of the air exiting the compressor

$$T_{\text{cp}} = T_{\text{atm}} + \frac{T_{\text{atm}}}{\eta_{\text{cp}}} \left(\Pi^{\frac{\kappa-1}{\kappa}} - 1 \right) \tag{8}$$

can be calculated using the heat capacity ratio $\kappa = c_{\text{p}}/c_{\text{v}}$ for air and the ambient temperature T_{atm}. With the energy balance and a constant electric efficiency η_{el} of the compressor, the required electric power P_{cp} can be calculated using

$$P_{\text{cp}} = \frac{1}{\eta_{\text{el}} \eta_{\text{cp}}} \dot{m}_{\text{cp}} T_{\text{cp}} \left(\Pi^{\frac{\kappa-1}{\kappa}} - 1 \right). \tag{9}$$

The surge distance $s_d = \dot{m}_{cp} - \dot{m}_{sd} = \dot{m}_{cp} - f_{sd}(\Pi)$ is calculated as the mass flow difference between the current compressor mass flow $\dot{m}_{cp}$ and the surge limit mass flow for the given pressure ratio $\dot{m}_{sd}$.

4.2 Three Tank Model of Air Path

Similar to (Pukrushpan et al., 2004), a compressor is assumed to be connected to an adiabatic supply manifold (sm) and isothermal cathode (ca) and return (rm) manifolds, modeled as volumes. In the cathode and return manifold, the flow temperature has adapted to the constant stack temperature, i. e. $T_{st} = T_{ca} = T_{rm}$. Since no stack-internal physics is modeled, we assume flow of air as only species. Based on the mass and energy

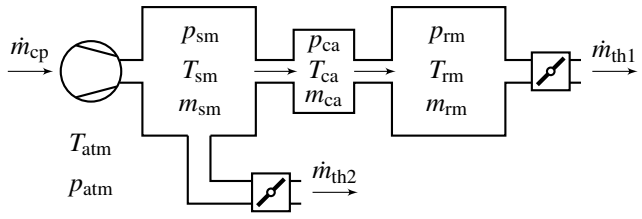

Fig. 1. Schematic of the three-tank model with bypass with state variables pressure p, temperature T and mass m.

balance, the adiabatic flow can be modeled. Neglecting external energy, the energy balance relates the change of internal energy $^{dU}/_{dt}$ to the enthalpy flow $\dot{m}h$ into and out of the volume.

$$\frac{dU}{dt} = \dot{m}_{in}h_{in} - \dot{m}_{out}h_{out} \tag{10}$$

For the pressure dynamics, using $U = mc_vT = \frac{pV}{\kappa - 1}$ and the ideal gas constant for air R_a, the equation reads as

$$\dot{p} = \frac{\kappa R_a}{V}(\dot{m}_{in}T_{in} - \dot{m}_{out}T_{out}). \tag{11}$$

For the isothermal flow, applying the ideal gas law to the mass balance yields the pressure dynamics

$$\dot{p} = \frac{R_aT}{V}(\dot{m}_{in} - \dot{m}_{out}). \tag{12}$$

the flow in-between volumes, i.e. $\dot{m}_{in}$ and $\dot{m}_{out}$, is modeled through the throttle equation for subcritical flow. The flow is driven by the pressure difference upstream p_u and downstream p_d of the throttle. If the throttle flow can be manipulated using one of the two throttles, an input dependent relation of the product of flow coefficient c_d and flow area A is modeled and denoted as $c_dA(u)$.

$$\dot{m} = \frac{c_dA(u)}{\sqrt{R_aT}}p_u\left(\frac{p_d}{p_u}\right)^{\frac{1}{\kappa}}\sqrt{\frac{2\kappa}{\kappa-1}\left(1-\left(\frac{p_d}{p_u}\right)^{\frac{\kappa-1}{\kappa}}\right)} \tag{13}$$

4.3 Stack Model

For the stack model, we assume a lumped stack with homogeneous temperature. The stack voltage $V_{st} = f(u, T_{st})$ is fitted as a static function of the inputs and the stack temperature. The stoichiometry λ of the lumped stack model is calculated using

$$\lambda = \frac{\dot{m}_{O_2}}{\dot{m}_{O_2,stoich}} = \frac{\dot{m}_{O_2}}{M_{O_2}\frac{n_{cell}I_{st}}{4F}}, \tag{14}$$

where n_{cell} is the number of cells in the stack and I_{st} the stack current. It relates the oxygen mass flow through the stack $\dot{m}_{O_2}$ to the mass flow need for stoichiometric operation $\dot{m}_{O_2,stoich}$. For computing $\dot{m}_{O_2,stoich}$, the molar mass of oxygen M_{O_2} and the Faraday constant F are used.

5. RESULTS

Closed loop simulations are conducted to evaluate the different CSS algorithms in terms of control performance and computational cost. We use the closed-loop cost

$$c = \frac{\sum_{i=0}^{t_{exp}} \|y_i - r_i\|_Q}{t_{exp}}, \tag{15}$$

for evaluating the control performance for an experiment of length t_{exp}, where the tracking error is weighted with the Q matrix and normalized by the number of time steps. All reported computation times result from numerical experiments on the rapid control prototyping (RCP) hardware board DS1401 equipped with a single-core PowerPC 750 GL processor running at 900 MHz and 16 MB flash memory. The algorithms are implemented in MATLAB/SIMULINK from which code is generated and compiled for the target. All QPs are solved with OSQP (Stellato et al., 2020) using default settings. The applied tuning parameters $\lambda_g = 10$, $\lambda_y = 10^4$, $Q = \mathrm{diag}(1,1,10)$ for $y = [s_d, \lambda, P_{net}]^T$, and $R = \mathrm{diag}(1,1,1,10)$ for $u = [n_{cp}, u_{th1}, u_{th2}, I_{st}]^T$ are found based on simulation studies.

5.1 Comparison of CSS algorithms

The initial data trajectory for the presented experiments leads to a Hankel matrix with $T - L + 1 = 2035$ columns. The resulting least-squares approximation error e and the closed-loop cost c are investigated for the different CSS algorithms described in Section 3 for a varying number of columns $n_c \in [80, 300]$, see Fig. 2 and Fig. 3. The least-squares error for the data set according to (7) is normalized by the error when using all data for calculating the optimal predictor in (6). Iterative norm sampling and sRRQR provide low errors even with few trajectories. Norm sampling leads to significantly larger errors than the ten randomly selected column combinations and leverage score sampling. For increasing n_c, all sampling algorithms converge to the same error.

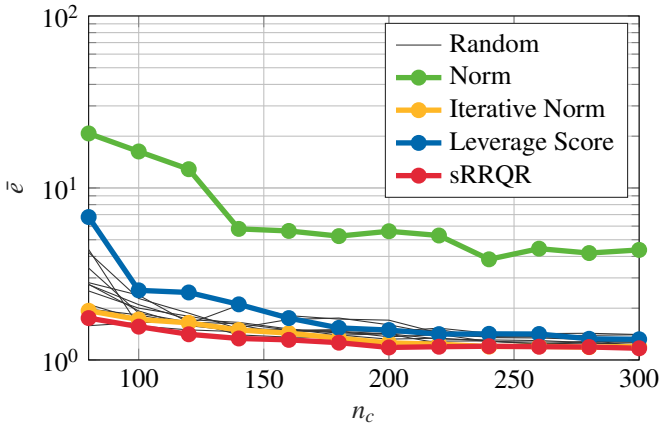

Fig. 2. Normalized least-squares error $\bar{e} = \|P^*_{n_c}M - Y_f\|_F^2 / \|P^*M - Y_f\|_F^2$ for different CSS algorithms and a varying number of selected columns n_c.

To further quantify the effect of the different CSS algorithms, closed-loop simulations with varying data matrices resulting

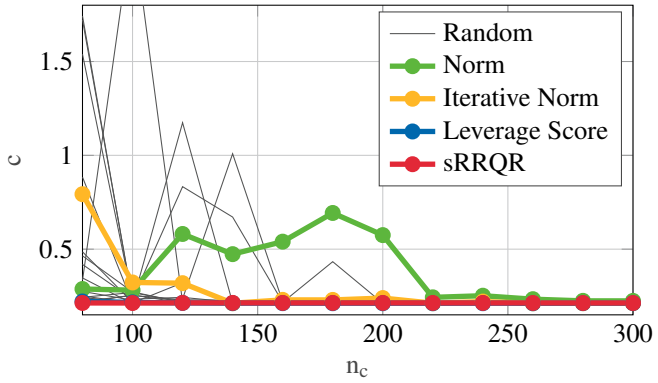

Fig. 3. Closed-loop cost according to (15) for different CSS strategies. Ten instances of random sampling are added for comparison.

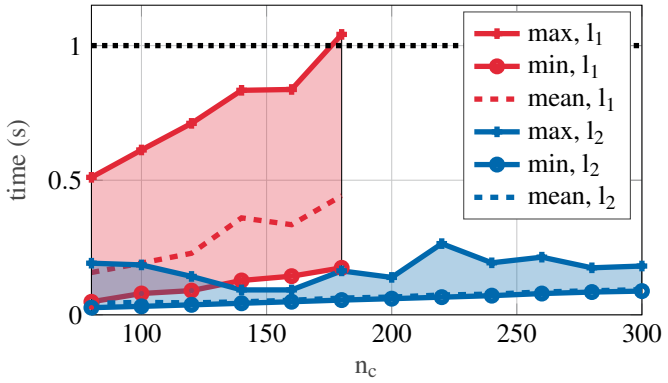

Fig. 4. Turnaround time for 1-norm and squared 2-norm regularization. The maximum, mean and minimum time for the reference cycle in Fig. 5 using leverage score as CSS algorithm is depicted.

from the CSS algorithms are conducted. Column selection by leverage scores and using the sRRQR algorithm provide low closed-loop cost for all tested n_c, especially for small n_c, with the sRRQR algorithm being slightly advantageous for $n_c = 80$. The difference in closed-loop is, however, small. Norm sampling leads to higher closed-loop cost for small n_c and the performance deteriorates for $n_c \in [120, 200]$ due to selection of too similar trajectories which do not cover the whole operating range. With the squared 2-norm penalty, this corresponds to overfitting a small operating range leading to impaired tracking, increased closed-loop cost and even constraint violations. As the number of sampled columns increases, the performance converges toward the result achieved with the sRRQR and leverage score algorithms. Iterative norm sampling leads to insufficient performance for a small number of columns selected, but quickly recovers for $n_c = 140$ to approximately the same closed-loop behavior as achieved with sRRQR and leverage score. Again, further increasing the number of columns does not automatically lead to monotonic decrease in closed-loop cost, but eventually, for $n_c \geq 220$, iterative norm sampling also converges to the same closed-loop cost.

For reference, random trajectory selections and the corresponding closed-loop cost are added to Fig. 3. With $n_c \geq 200$, the random selection always achieves satisfactory closed-loop tracking results, gathering enough trajectories to accurately predict the systems behavior. For a lower number of trajectories, corresponding to a lower memory footprint and smaller computation times, the closed-loop control results of random sampling have a wider distribution of closed-loop cost. Closed-loop control results are less predictable for different random realizations of the column subset selection, which is therefore less suitable for potential online updates of the data matrix.

Comparing Fig. 2 and Fig. 3, we conclude that the least-squares approximation error is only an indicator and not a predictor of closed-loop cost. It significantly depends on a balanced data set covering all relevant operating conditions evenly. While for sRRQR and norm sampling, the results are consistent, closed-loop cost for iterative norm sampling and leverage score sampling do not match the least-squares result.

5.2 Complexity of 1-norm and squared 2-norm penalty

In a next simulation study, the effects on turnaround time and closed-loop control of penalizing g with the 1-norm and with the squared 2-norm are investigated. Using the leverage score sampling and a varying number $n_c \in [80, 300]$ of selected columns, minimum, maximum, and mean turnaround times are depicted in Fig. 4. While all results using the squared 2-norm are well below the sampling time of $T_s = 1\,\mathrm{s}$, the reformulation of the 1-norm with more optimization variables leads to a significant increase in minimum, average, and worst-case computation time. For $n_c > 160$, real-time computations cannot be achieved anymore on the given hardware. In closed-loop control, however, no significant difference was found. Closed-loop control results are depicted in Fig. 5 for $n_c = 80$, using the 1-norm and squared 2-norm with sRRQR sampling, and random sampling with squared 2-norm penalty on g. Both regularization schemes lead to suitable and comparable reference tracking. Because of similar closed-loop tracking with fewer optimization variables, the squared 2-norm penalty is used in the following.

5.3 Control Results

The DeePC controller is evaluated for a power reference cycle. Surge distance and stoichiometry should track a constant reference for efficiency. In addition, for safe operation, both the surge distance and the stoichiometry are constrained. Using the results from the previous section, the controller is evaluated at $n_c = 80$ employing the sRRQR algorithm for column subset selection. Both 1-norm and squared 2-norm penalty are depicted in Fig. 5 and yield similar closed-loop tracking of all outputs. Specifically, the power tracking is accurate and fast, while the stoichiometry and the surge distance remain close to the reference and within the safe operation regime. Out of ten random column samplings with $n_c = 80$, seven simulations result in no or minor constraint violations and significantly higher closed-loop costs. Those results are added to Fig. 5. The remaining three random sampling instances lead to oscillations and numerous constraint violations and are removed from the plot for readability. This reveals that a small number of columns, in our case $n_c = 80$, can be sufficient to accurately describe the system behavior. Reliably detecting the relevant columns in the initial data matrix is therefore a crucial task that can be tackled using the sRRQR algorithm for column subset selection.

6. CONCLUSION

The DeePC algorithm is applied to a fuel cell system. For practical application, algorithmic choices such as the penalty

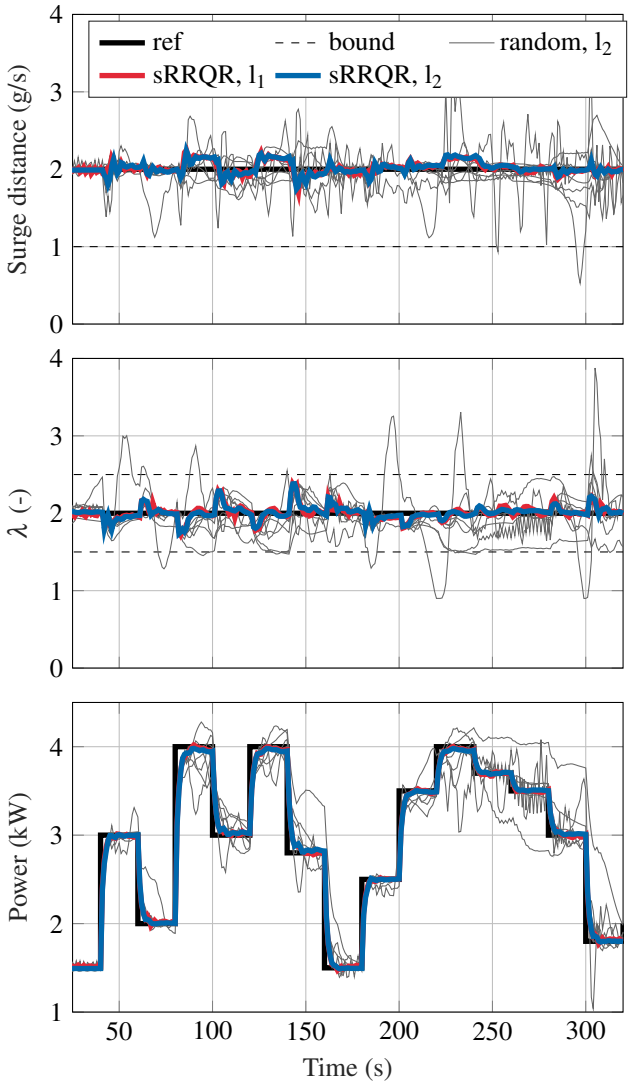

Fig. 5. Closed-loop control result for the DeePC controller using $n_c = 80$ columns from the original data matrix and the sRRQR algorithm. Regularization with the 1- and the squared 2-norm lead to similar close-loop behavior. Random sampling results in oscillations, high closed-loop cost or even control failure through constraint violations.

on g and different methods for column subset selection of an initially large Hankel matrix are investigated. It is found that penalizing g with the squared 2-norm is advantageous because of a smaller resulting QP and therefore faster computation times with comparable closed-loop performance. Out of the investigated column subset selection algorithms, sRRQR and leverage score sampling showed good closed-loop tracking results, even with fewer columns which reduces the number of variables and the overall turnaround time. Future work will build on these results to develop an online adaption in terms of exchanging columns from the data matrix to update the data model.

ACKNOWLEDGEMENTS

The research project was carried out in the framework of the industrial collective research program (IGF no. 61 EWN). It was supported by the Federal Ministry for Economic Affairs and Climate Action (BMWK) through the AiF (German Federation of Industrial Research Associations eV) based on a decision taken by the German Bundestag.

REFERENCES

Berberich, J., Köhler, J., Müller, M., and Frank Allgöwer, F. (2020). Robust constraint satisfaction in data-driven MPC. *59th IEEE Conference on Decision and Control (CDC)*.

Berberich, J., Köhler, J., Müller, M., and Frank Allgöwer, F. (2021a). Data-driven model predictive control: closed-loop guarantees and experimental results. *at - Automatisierungstechnik*, 69, 608–618.

Berberich, J., Köhler, J., Müller, M., and Frank Allgöwer, F. (2021b). On the design of terminal ingredients for data-driven mpc. *IFAC-PapersOnLine*, 54, 257–263.

Carlet, P.G., Facato, A., Bolognani, S., and Dörfler, F. (2020). Data-driven predictive current control for synchronous motor drives. *IEEE Energy Conversion Congress and Exposition (ECCE)*, 5148–5154.

Chan, T.F. (1987). Rank revealing qr factorizations. *Linear Algebra and its Applications*, 88–89, 67–82.

Coulson, J., Lygeros, J., and Dörfler, F. (2019a). Data-enabled predictive control for grid-connected power converters. *58th IEEE Conference on Decision and Control (CDC)*, 8130–8135.

Coulson, J., Lygeros, J., and Dörfler, F. (2019b). Data-enabled predictive control: In the shallows of the deepc. *18th European Control Conference (ECC)*, 307–312.

Coulson, J., Lygeros, J., and Dörfler, F. (2019c). Regularized and distributionally robust data-enabled predictive control. *58th Conference on Decision and Control (CDC)*, 2696–2701.

Coulson, J., Lygeros, J., and Dörfler, F. (2020). Distributionally robust chance constrained data-enabled predictive control.

Elokda, E., Coulson, J., Beuchat, P., Lygeros, J., and Dörfler, F. (2019). Data-enabled predictive control for quadrocopters.

Fiedler, F. and Lucia, S. (2020). On the relationship between data-enabled predictive control and subspace predictive control.

Gu, M. and Eisenstat, S.C. (1996). Efficient algorithms for computing a strong rank-revealing qr factorization. *SIAM Journal on Scientific Computing*, 848–869.

Hou, Z. and Wang, Z. (2013). From model-based control to data-driven control: Survey, classification and perspective. *Information Sciences*, 235, 3–35.

Markovsky, I. and Rapisarda, P. (2008). Data-driven simulation and control. *International Journal of Control*, 81, 1946–1959.

Pukrushpan, J.T., Peng, H., and Stefanopoulou, A.G. (2004). Control-oriented modeling and analysis for automotive fuel cell systems. *Journal of Dynamic Systems, Measurement, and Control*, 126.

Stellato, B., Banjac, G., Goulart, P., Bemporad, A., and Boyd, S. (2020). OSQP: an operator splitting solver for quadratic programs. *Mathematical Programming Computation*, 12, 637–673.

Wang, Y. and Singh, A. (2015). An empirical comparison of sampling techniques for matrix column subset selection. *53rd Annual Allerton Conference on Communication, Control, and Computing*, 1069–1074.

Willems, J.C., Rapisarda, P., Markovsky, I., and De Moor, B.L. (2005). A note on persistency of excitation. *Systems & Control Letters*, 54, 325–329.